

Article

N-S Asymmetry and Solar Cycle Distribution of Superactive Regions from 1976 to 2017

Ming-Xian Zhao ¹, Gui-Ming Le ^{1,2,3,4,*} and Yong-Hua Liu ⁵

¹ Key Laboratory of Space Weather, National Satellite Meteorological Center (National Center for Space Weather), China Meteorological Administration, Beijing 100081, China

² School of Physics Science & Technology, Lingnan Normal University, Zhanjiang 524048, China

³ Innovation Center for FengYun Meteorological Satellite (FYSIC), Beijing 100081, China

⁴ Key Laboratory of Solar Activity, National Astronomical Observatories, Chinese Academy of Sciences, Beijing 100012, China

⁵ Polar Research Institute of China, Shanghai 200136, China

* Correspondence: legm@cma.gov.cn

Abstract: There were 51 superactive regions (SARs) during solar cycles (SCs) 21–24. We divided the SARs into SARs₁, which produced extreme space weather events including $\geq X5.0$ flares, ground level events (GLEs), and super geomagnetic storms (SGSs, $Dst < -250$ nT), and SARs₂, which did not produce extreme space weather events. The total number of SARs₁ and SARs₂ are 31 and 20, respectively. The statistical results showed that 35.5%, 64.5%, and 77.4% of the SARs₁ appeared in the ascending phase, descending phase, and in the period from two years before to the three years after the solar maximum, respectively, whereas 50%, 50%, and 100% of the SARs₂ appeared in the ascending phase, descending phase, and in the period from two years before to the three years after the solar maximum, respectively. The total number of SARs during an SC has a good association with the SC amplitude, implying that an SC with a higher amplitude will have more SARs than that with a lower amplitude. However, the largest flare index of a SAR within an SC has a poor association with the SC amplitude, suggesting that a weak cycle may have a SAR that may produce a series of very strong solar flares. The analysis of the north–south asymmetry of the SARs showed that SARs₁ dominated in the southern hemisphere of the sun during SCs 21–24. The SAR₂ dominated in the different hemispheres by turns for different SCs. The solar flare activities caused by the SARs with source locations in the southern hemisphere of the sun were much stronger than those caused by the SARs with source locations in the northern hemisphere of the sun during SCs 21–24.

Keywords: sunspots; flares; particle emission; solar–terrestrial relations



Citation: Zhao, M.-X.; Le, G.-M.; Liu, Y.-H. N-S Asymmetry and Solar Cycle Distribution of Superactive Regions from 1976 to 2017. *Universe* **2022**, *8*, 605. <https://doi.org/10.3390/universe8110605>

Academic Editors: Jie Chen, Yuandeng Shen, Marianna Korsos and Robertus Erdelyi

Received: 21 September 2022

Accepted: 15 November 2022

Published: 17 November 2022

Publisher's Note: MDPI stays neutral with regard to jurisdictional claims in published maps and institutional affiliations.



Copyright: © 2022 by the authors. Licensee MDPI, Basel, Switzerland. This article is an open access article distributed under the terms and conditions of the Creative Commons Attribution (CC BY) license (<https://creativecommons.org/licenses/by/4.0/>).

1. Introduction

There are generally a large number of active regions (ARs) during a solar cycle. However, only a small number of ARs, which are defined as superactive regions (SARs), can produce very strong solar activities. A SAR is a special AR, which usually produces more and stronger solar flares than those ARs that are not SARs. The soft X-ray flare index of an AR is the sum of the numerical multipliers of M and X class X-ray flares for the disk transit of the AR, e.g., 0.1 for an M1 class flare and 1.0 for an X1 class flare. The criteria of a SAR proposed by different researchers were a little different [1–3]. If an AR satisfies the four conditions, including the largest area $> 1000 \mu\text{h}$, the flare index > 10 , the peak flux of $10.7 \text{ cm} > 1000 \text{ s.f.u.}$, and the short-term total solar irradiance decrease $< -0.1\%$, then the AR is defined as a SAR, as proposed by Chen et al. [3]. The comparison among the criteria proposed by different researchers have been made by Chen et al. [3] and by Le et al. [4]. According to the criteria proposed by Chen et al. [3], the SAR 12673 that occurred in September 2017 is also a SAR. The total number of SARs during SCs 21–23, which were listed in the appendix of the article by Chen et al. [3] is 45, and the

number of the SARs during SC 24 includes the five SARs listed in the article by Chen and Wang [5] and the SAR 12673 is 6. Thus, the total number of SARs during SCs 21–24 is 51. Solar soft X-ray flares with intensities $\geq X5.0$, ground-level events (GLEs), and super geomagnetic storms (SGSs, $Dst < -250$ nT) are defined as extreme space weather events in this study. It was found that some SARs produced extreme space weather events [4,6], whereas other SARs did not produce extreme space weather events. According to whether a SAR produced extreme space weather events, we divided the SARs into two subgroups: SARs₁, which produced extreme space weather events, and SARs₂, which did not produce extreme space weather events.

The solar cycle distribution of various solar activities, solar wind, and space weather phenomena has been studied (e.g., [6–11]). What is the pattern of the solar cycle distribution of the SARs₁ and SARs₂ from 1976 to 2017? To answer the question, the SC distribution of the two subgroups of the SARs from 1976 to 2017 will be studied. The north–south (N–S) asymmetry of various parameters is an important property of solar activities. Solar activities in the two hemispheres of the sun are controlled by the dynamo actions in the two hemispheres of the sun. The N–S asymmetry can be used to check or verify whether the dynamo action in the two hemispheres is synchronized or whether there exists observational evidence for differences in the dynamo action in the two hemispheres [12], indicating that the study of the N–S asymmetries of solar activities is very important. The N–S asymmetries of the various solar activities such as solar flares, solar flares index, and sunspot activities have been extensively studied (e.g., [13–30] and references therein). The N–S asymmetry of the SARs was studied by Chen et al. However, the N–S asymmetry of SARs₁ and SARs₂ has not been studied. What is the pattern of the N–S asymmetry of the SARs₁ and SARs₂ from 1976 to 2017? To answer the question, the N–S asymmetry of the SARs₁ and SARs₂ from 1976 to 2017 will be studied. Duchlev [31] found a long-term period of about 11 solar cycles in the filament asymmetry variation by using the cumulative index for the filament N–S asymmetry. N–S asymmetry of the cumulative index for many solar activities has been studied (e.g., [20,32,33]). The N–S asymmetry of the cumulative numbers of the SARs in the northern and southern hemispheres of the sun will be investigated in this study. The N–S asymmetry of the solar flare activities caused by the SARs in the northern and southern hemispheres of the sun will also be studied. The relationship between the number of SARs and the SC amplitude will be studied. The relationship between the SC amplitude and the largest flare index caused by a SAR will be studied. The rest part of the article is organized as follows. Section 2 is data analysis. Section 3 is a summary and discussion.

2. Data Analysis

2.1. Data Source

The smoothed monthly mean sunspot numbers (SMMSNs) were obtained from the following website: <http://sidc.oma.be/silso/datafiles> (accessed on 1 June 2022). The flares with intensities $\geq X5.0$ during SCs 21–24 were obtained from the website <ftp://ftp.ngdc.noaa.gov/STP/space-weather/solar-data/solar-features/solar-flares/x-rays/goes/xrs/> (accessed on 1 June 2022). The Dst index were acquired from the website at <http://wdc.kugi.kyoto-u.ac.jp/> (accessed on 1 June 2022). The GLEs were obtained from the website at <https://gle oulu.fi/> (accessed on 1 June 2022).

2.2. Solar Cycle Distribution of the SARs from 1976 to 2017

SMMSNs are usually used to describe the solar cycle. The period from the first month of a solar cycle to the month when the SMMSNs reach their maximum is defined as the ascending phase of the solar cycle (SC). The period from one month after the maximum of the SMMSNs to the last month of the SC is defined as the descending phase of the SC. The SARs₁ and SARs₂ were selected from the article by Le et al. [4]. According to the article by Le et al. [4], 51 SARs and the extreme space weather caused by the corresponding SARs₁ were compiled and listed in Table A1 of the appendix. According to Table A1 and the new series of SMMSNs launched on 1 July 2015, the SC distribution of the SARs₁ and

SARs₂ from 1976 to 2017 is shown in Figure 1. The numbers of SARs₁ and SARs₂ during different periods of an SC, and the statistical results during SCs 21–24 were listed in Table 1. In Table 1, N_a , N_d and N_{23} indicate the numbers of the SARs that occurred during the ascending phase, the descending phase, and the period from two years before to three years after the solar maximum for each SC, respectively. N_t indicates the total number of SARs during an SC, i.e. $N_t = N_a + N_d$. The largest SMMSNs in an SC were defined as the SC amplitude in this study. In Table 1, N_{sa} , N_{sd} , N_{s23} , and N_{st} indicate the sum of N_a , N_d and N_{23} and N_t during SCs 21–24. The derived N_{sa}/N_{st} , N_{sd}/N_{st} and N_{s23}/N_{st} for SARs₁ are 35.5%, 64.5% and 80.6%, respectively. The derived N_{sa}/N_{st} , N_{sd}/N_{st} and N_{s23}/N_{st} for SARs₂ are 50%, 50%, and 100%, respectively. The results of the SC distribution showed that most of the SARs appeared around solar maximum.

The flare index (FI) caused by each SAR is directly copied from the article by Chen et al. [3] and the article by Chen and Wang [5]. The FI caused by SAR 12673 is calculated according to the calculation method recommended in the article by Chen et al. [3]. For the convenience of the description, we use SAR_{max} to indicate the SAR that has the largest FI during an SC. As shown in Figure 1, the SAR_{max} of each SC always occurred in the descending phase of the SC.

Table 1. Solar cycle distribution of SARs from 1976 to 2017.

SC	SC Amplitude	SARs ₁				SARs ₂			
		N_a	N_d	N_{23}	N_t	N_a	N_d	N_{23}	N_t
21	232.9	1	8	7	9	4	4	8	8
22	212.5	4	6	10	10	3	3	6	6
23	180.3	5	5	5	10	0	2	2	2
24	116.4	1	1	2	2	3	1	4	4
Total number		$N_{sa} = 11$	$N_{sd} = 20$	$N_{s23} = 24$	$N_{st} = 31$	$N_{sa} = 10$	$N_{sd} = 10$	$N_{s23} = 20$	$N_{st} = 20$

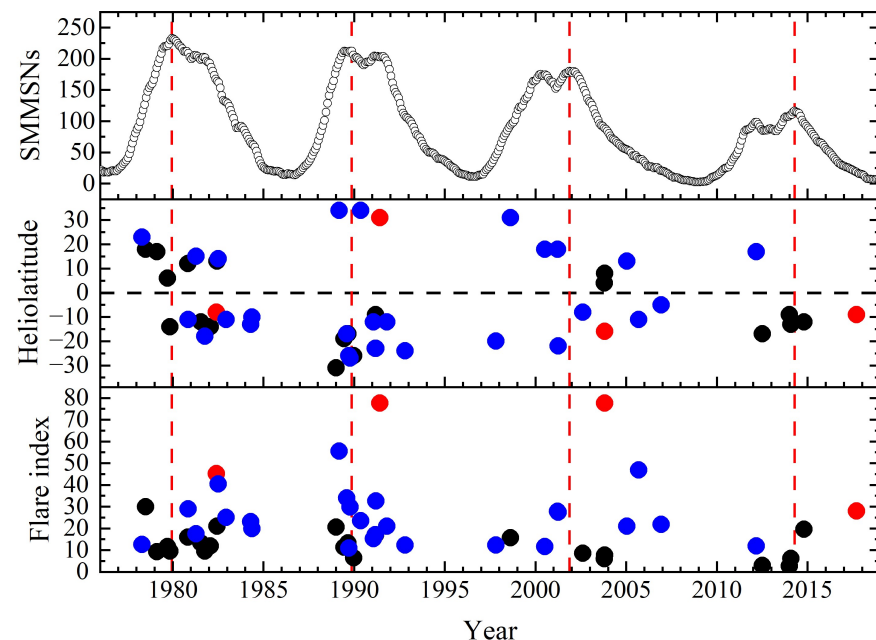


Figure 1. SC distribution of SARs from 1976 to 2017. From the top to bottom, it shows SMMSNs, the heliolatitude of the SARs, and the FI of the SARs. The black solid circles indicate the SARs₂, whereas the blue and red solid circles indicate the SARs₁. The red solid circles indicate the SARs that have the largest FI in each SC. The red vertical dashed lines indicate the peak times of the four SCs, respectively.

The correlation coefficient (CC) between the total number of SARs within an SC and the SC amplitude is calculated, and the statistical significance (SS) of the CC is also estimated and shown in the right panel of Figure 2. Statistical significance means that it is unlikely to have occurred by chance, and the results are reliable when the percentage of statistical significance is above 95%. As shown in Figure 2, the CC between the total number of SARs within an SC and the SC amplitude is 0.996 and the SS is over 95%, indicating that the total number of SARs within an SC has a good correlation with the SC amplitude. The derived CC between the largest FI caused by a SAR during an SC and the SC amplitude is 0.50 (shown in the left panel of Figure 2). The SS for the derived CC is lower than 95% (shown in the left panel of Figure 2), indicating that the largest FI of a SAR_{max} during an SC has a poor correlation with the SC amplitude.

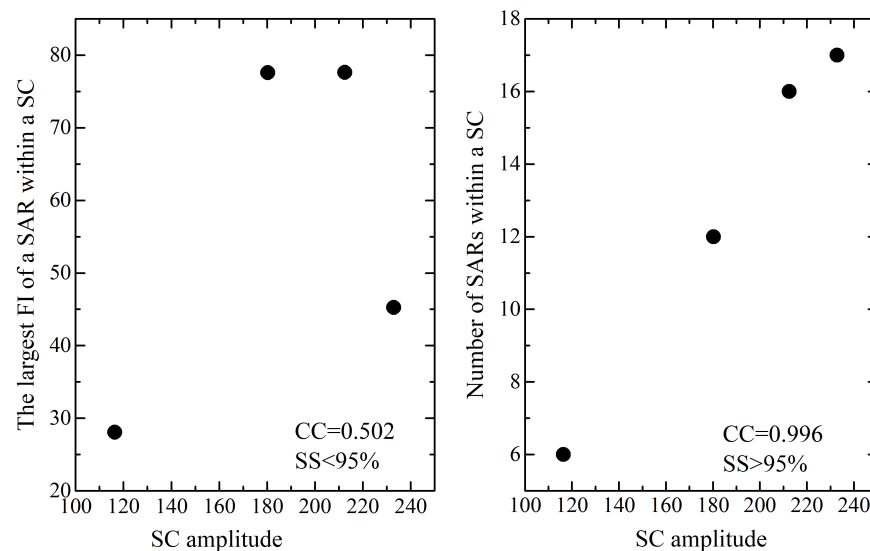


Figure 2. The correlation between the largest FI of a SAR within an SC and the SC amplitude on the left panel, and the correlation between the number of SARs within an SC and the SC amplitude on the right panel.

2.3. N–S Asymmetry

To study the N–S asymmetry of SARs₁ and SARs₂ during SCs 21–24, the numbers of SARs₁ and SARs₂ in the two hemispheres of the sun during each SC are listed in Table 2. In Table 2, we use N and S to indicate the number of SARs in the northern and southern hemispheres of each SC, respectively. We can see from Table 2 that the SARs₁ dominated in the southern hemisphere of the Sun during SCs 21–23, whereas N–S is equal to zero in SC 24. The SARs₁ in the northern and southern hemispheres of the sun were SAR 11429 and SAR 12673, respectively. The FI caused by SAR 12673 was 28.06, whereas the FI caused by SAR 11429 was 11.87. It is evident that the FI caused by AR 12673 was much larger than that caused by SAR 11429. As shown in the appendix, SAR 12673 produced an X9.2 and an X8.3 flare. In addition, SAR 12673 produced a GLE event. The flare stronger than X5 caused by SAR 11429 was an X5.9. These indicate that the solar activities caused by SAR 12673 were stronger than that caused by SAR 11429. In this context, the SARs₁ mainly appeared in the southern hemisphere of the sun during SCs 21–24, i.e., the extreme space weather events were mainly produced by the SARs from the southern hemisphere of the sun during SCs 21–24. As shown in Table 2, the SARs₂ dominated in the northern hemisphere during SCs 21 and 23, whereas the SARs₂ dominated in the southern hemisphere during SCs 22 and 24.

Table 2 is the comparison between the number of SARs₁ and SARs₂ from two hemispheres of the sun. To further compare the solar activities caused by the SARs with source locations in the two different hemispheres, we use $\sum_{SARs} FI_n$ and $\sum_{SARs} FI_s$ to indicated the

sums of the FI caused by the SARs with source locations in the northern and southern hemispheres of the sun, respectively. The $\sum_{SARs} FI_n$ and $\sum_{SARs} FI_s$ during the ascending phase, descending phase and the whole SC from 1976 to 2017 were derived and shown in Table 3. We can see from Table 3 that the sum of the flare indices caused by the SARs with source locations in the northern hemisphere was larger than that caused by the SARs with source locations in the southern hemisphere of the sun during the ascending phases for SCs 21, 23, and 24. The sum of the flare indices caused by the SARs with source locations in the southern hemisphere was larger than that caused by the SARs with source locations in the northern hemisphere of the sun during the ascending phases of SC22. As shown in Table 3, the activities of the solar flares caused by the SARs with source locations in the southern hemisphere were always stronger than those caused by the SARs with source locations in the northern hemisphere during the descending phase for SCs 21–24. We can also see from Table 3 that the total flare indices during a whole SC caused by the SARs with source locations in the southern hemisphere were slightly stronger than those in the northern hemisphere of the sun for SC21, whereas the total flare indices during a whole SC caused by the SARs with source locations in the southern hemisphere were always much stronger than those caused by the SARs with source locations in the northern hemisphere of the sun for SCs 22–24.

Table 2. The number of SARs₁ and SARs₂ in the two hemispheres and their difference during each SC.

SC	SARs ₁			SARs ₂		
	N	S	N–S	N	S	N–S
21	3	6	–3	5	3	2
22	3	7	–5	0	6	–5
23	4	6	–2	2	0	2
24	1	1	0	0	4	–4

Table 3. The comparison $\sum_{SARs} FI_n$ and $\sum_{SARs} FI_s$ for different periods of solar cycles.

SC	Ascending Phase		Descending Phase		Total SC	
	$\sum_{SARs} FI_n$	$\sum_{SARs} FI_s$	$\sum_{SARs} FI_n$	$\sum_{SARs} FI_s$	$\sum_{SARs} FI_n$	$\sum_{SARs} FI_s$
21	63.3	9.5	94.82	177.1	158.12	186.6
22	55.6	120.06	101.12	121.6	156.72	241.66
23	55.27	39.7	21.06	168.62	76.33	208.32
24	11.87	11.73	0	47.65	11.87	59.38

According to Table 2, the cumulative numbers of the SARs₁ and SARs₂ during different periods, which include a different number of SCs, are shown in Table 4. A Student’s t-test is a statistical test for a noninteger and dimensional time series [17], which is used to test the statistical significance of the N–S asymmetries of the difference for both the number and the cumulative number of the SARs in the northern and southern hemispheres of the sun during the period from SC 21 to SC 24. The Student’s t-test is also used to test the statistical significance of the N–S asymmetry of the flare indices caused by the SARs in the northern and southern hemispheres of the sun during the period from SC 21 to SC 24 shown in 3. The Student’s t-test values are set at a 95% probability level. We found that the N–S asymmetries of both the number and the cumulative number of the SARs₁ during SCs 21–24 shown in Table 4 are significant, whereas the N–S asymmetry of the cumulative numbers of the SARs₂ during SCs 21–24 shown in Table 4 is not significant. The N–S asymmetry of the flare indices caused by the SARs from the southern and the northern hemispheres of the sun during SCs 21–24 shown in Table 3 is significant.

Table 4. The cumulative number of SARs₁ and SARs₂ during SCs 21–24

SC	SARs ₁			SARs ₂		
	N	S	N–S	N	S	N–S
21	3	6	–3	5	3	2
21–22	6	14	–8	5	8	–3
21–23	10	20	–10	7	8	–1
21–24	11	21	–11	7	12	–5

3. Summary and Discussion

The main results are summarized as follows:

- (i) There were 51 SARs during SCs 21–24. Of the 51 SARs, 31 SARs belong to SARs₁ and 20 SARs are SARs₂. The statistical results show that N_{sa}/N_{st} , N_{sd}/N_{st} and N_{s23}/N_{st} of SARs₁ are 35.5%, 64.5% and 77.4%, respectively, whereas N_{sa}/N_{st} , N_{sd}/N_{st} and N_{s23}/N_{st} for SARs₂ are 50%, 50%, and 100%, respectively, indicating that most of the SARs appeared around the solar maximum, which is very similar to those of strong solar proton events [11], major geomagnetic storms [6] and GLEs [10]. It has been found that stronger storms have the tendency to occur around the solar maximum [9,33]. The SAR that produced the largest FI during each SC always occurred in the descending phase of the SC.
- (ii) The number of the SARs during an SC has a good correlation with the SC amplitude, implying that an SC with higher amplitude will have more SARs than that with lower amplitude. However, the largest FI of a SAR during an SC has a poor correlation with the SC amplitude, indicating that a weak SC will have a small number of SARs. However, a weak SC may have a SAR that can produce very strong solar flares. It has been predicted that SC 25 may be a weak SC [34–36], implying that the total number of SARs in SC 25 will be small. However, we cannot rule out the possibility that SC 25 may have a SAR that can produce a series of very strong solar activities, including flares and CMEs, and then cause GLEs and even extreme geomagnetic storms.
- (iii) N–S asymmetries of both the number and cumulative number of SARs₁ in the two different hemispheres of the sun during the period from SC 21 to SC 24 are significant, i.e., the SARs₁ dominated in the southern hemisphere of the sun during the period from SC 21 to SC 24. This indicated that the extreme solar activities and space weather events during the periods from SC 21 to SC 24 were mainly caused by the SARs₁ in the southern hemisphere of the sun. However, the N–S asymmetry of the SARs₂ during the period from SC 21 to SC 24 is not significant, i.e., the SAR₂ dominated in the different hemispheres by turns for different SCs. N–S asymmetry of the flare indices caused by the SARs from the two different hemispheres of the Sun during the period from SC 21 to SC 24 is inferred to exist. The solar flare activities caused by the SARs with source locations in the southern hemisphere of the sun were much stronger than those caused by the SARs with source locations in the northern hemisphere of the sun during SCs 21–24.

Author Contributions: M.-X.Z. compiled the manuscript with Latex; G.-M.L.: providing the idea, making calculations needed for the study, plotting the figure, writing the manuscript with MS Word, checking and revising the manuscript; Y.-H.L.: polishing the English of the manuscript and paying the fee for the article publication. All authors took part in, discussed, and agreed on the results of the calculations. All authors have read and agreed to the published version of the manuscript.

Funding: This work is jointly supported by Sino–South Africa Joint Research on Polar Space Environment (2021YFE0106400), International Cooperation Project on Scientific and Technological Innovation between Governments, National Key Plans on Research and Development, Ministry of Science and Technology, China, and CAS Key Laboratory of Solar Activity under number KLSA (grant No. KLSA202109), and the National Natural Science Foundation of China (Grant No. 41074132, 41274193, 41674166).

Data Availability Statement: The authors thank Solar Influences Data Analysis Center for it provides smoothed monthly mean sunspot numbers at <http://sidc.oma.be/silso/datafiles> (accessed on 1 June 2022). The geomagnetic field data used in this paper was provided by the WDC for Geomagnetism, Kyoto (<http://wdc.kugi.kyoto-u.ac.jp/wdc/Sec3.html> (accessed on 1 June 2022)). The flares with intensities $\geq X5.0$ during SCs 21–24 were obtained from the website <ftp://ftp.ngdc.noaa.gov/STP/space-weather/solar-data/solar-features/solar-flares/x-rays/goes/xrs/> (accessed on 1 June 2022).

Conflicts of Interest: The authors declare no conflict of interest.

Appendix A

The total number of SARs during solar cycles 21–24 is 51, which are listed in Table A1. In the table, columns 1–9 are sequential number, the SC, the NOAA number of the SAR, $\geq X5.0$ flares caused by the SAR, latitude of the SAR, CL of the SAR, GLE No., SGS caused by the SAR, respectively. The shorter horizontal line in the table is the dividing line between the ascending and descending phases of the corresponding SC.

Table A1. The 51 SARs during SCs 21–24 and their extreme space weather events.

No.	SC	SAR	Latitude	CL	Date on the Disk yymmdd–mmdd	$\geq X5.0$ Flare	FI	GLE No.	SGSs
1		1092	N23	L081	780423–0507	X5.0	12.6		
2		1203	N18	L175	780708–0721		29.9		
3		1574	N17	L155	790214–0225		9.2		
4		1994	N06	L198	790916–0927		11.6		
5		2099	S14	L283	791105–1112		9.5		
6	21	2776	N12	L174	801101–1114		15.91		
7		2779	S11	L105	801105–1119	X9.0	29.03		
8		3049	N15	L153	810414–0430	X5.9 + X5.5	17.5		
9		3234	S12	L294	810721–0803		13.28		
10		3390	S18	L339	811007–1019		9.57	36	
11		3576	S14	L322	820126–0209		11.94		
12		3763	S08	L086	820602–0615	X8.0 + X5.9	45.24		
13		3776	N13	L314	820611–0624		20.94		
14		3804	N14	L322	820708–0722	X9.8 + X7.1	40.47		–325 nT
15		4026	S11	L078	821211–1223	X12.9 + X5.0	25.04		
16		4474	S13	L343	840421–0505	X13.0	23.13		
17		4492	S10	L358	840518–0531	X10.1	19.87		
18	22	5312	S31	L306	890106–0120		20.64		
19		5395	N34	L256	890305–0319	X15.0 + X6.5	55.6		–589 nT
20		5533	S19	L073	890609–0620		11.37		
21		5629	S17	L075	890803–0817	X20.0	34.07	41	
22		5669	S17	L085	890829–0912		13.32		
23		5698	S26	L220	890918–0929	X9.8	10.97		
24		5747	S27	L210	891014–1027	X13.0 + X5.7	29.87	43 + 44 + 45	–268 nT
25		5852	S26	L028	891225–1231		6.42		
26		6063	N34	L318	900511–0524	X5.5 + X9.3	23.51	47 + 48 + 49 + 50	
27		6471	S12	L144	910125–0208	X10.0	15.27		
28		6538	S23	L342	910305–0317	X5.5	17.08		
29		6545	S09	L287	910311–0322		16.93		
30		6555	S23	L188	910317–0331	X9.4 + X5.3	32.62		–298 nT
31		6659	N31	L247	910601–0617	5(X12.0) + X10.0	77.61	51 + 52	
32		6891	S12	L184	911021–1102	X6.1	20.96		–254 nT
33		7321	S24	L070	921025–1102	X9.0	12.32	54	

Table A1. Cont.

No.	SC	SAR	Latitude	CL	Date on the Disk yymmdd–mmdd	\geq X5.0 Flare	FI	GLE No.	SGSs
34	23	8100	S20	L352	971028–1107	X9.4	12.28	55	
35		8307	N31	L035	980818–0831		15.75	58	
36		9077	N18	L310	000709–0719	X5.7	11.68	59	–301 nT
37		9393	N18	L153	010324–0404	X20.0	27.84		–387 nT
38		9415	S22	L359	010403–0416	X5.6 + X14.4	27.42	60 + 61	–271 nT
39		10069	S08	L299	020811–0824		8.51	64	
40		10484	N04	L354	031018–1028		6.01		
41		10486	S16	L284	031022–1105	X5.4 + X17.2 + X10 + X8.3 + X28	77.56	65 + 66 + 67	(–383nT) + (–353nT)
42		10488	N08	L290	031027–1104		7.78		
43		10720	N13	L179	050111–0123	X7.1	21.06	68 + 69	
44		10808	S11	L230	050907–0918	X17.0 + X5.4 + X6.2	46.92		
45		10930	S05	L009	061204–1218	X9.0 + X6.5	21.84	70	
46	24	11429	N17	L081	120303–0315	X5.9	11.87		
47		11520	S17	L084	120706–0717		2.92		
48		11944	S09	L100	140101–0113		2.68		
49		11967	S13	L114	140128–0209		6.13		
50			12192	S12	L248	141017–1030		19.59	
51		12673	S09	L117	170830–0910	X9.2 + X8.3	28.06	72	

Noted: Bold words indicate that the SARs belong to SARs₁.

References

- Bai, T. Distribution of flares on the sun-Superactive regions and active zones of 1980–1985. *Astrophys. J.* **1987**, *314*, 795–807. [\[CrossRef\]](#)
- Tian, L.; Liu, Y.; Wang, J. The Most Violent Super-Active Regions in the 22nd and 23rd Cycles. *Sol. Phys.* **2002**, *209*, 361–374. [\[CrossRef\]](#)
- Chen, A.; Wang, J.; Li, J.; Feynman, J.; Zhang, J. Statistical properties of superactive regions during solar cycles 19–23. *A&A* **2011**, *534*, A47. [\[CrossRef\]](#)
- Le, G.M.; Liu, G.A.; Zhao, M.X.; Mao, T.; Xu, P.G. Extreme space weather events caused by super active regions during solar cycles 21–24. *Res. Astron. Astrophys.* **2021**, *21*, 130. [\[CrossRef\]](#)
- Chen, A.; Wang, J. Super-active regions in solar cycle 24. *Proc. Int. Astron. Union* **2015**, *11*, 309–314. [\[CrossRef\]](#)
- Le, G.M.; Zhao, M.X.; Zhang, W.T.; Liu, G.A. Source Locations and Solar-Cycle Distribution of the Major Geomagnetic Storms (Dst \leq –100 nT) from 1932 to 2018. *Sol. Phys.* **2021**, *296*, 187. [\[CrossRef\]](#)
- Richardson, I.G.; Berdichevsky, D.; Desch, M.D.; Farrugia, C.J. Solar-cycle variation of low density solar wind during more than three solar cycles. *Geophys. Res. Lett.* **2000**, *27*, 3761–3764. [\[CrossRef\]](#)
- Tokumaru, M.; Kojima, M.; Fujiki, K. Solar cycle evolution of the solar wind speed distribution from 1985 to 2008. *J. Geophys. Res. Space Phys.* **2010**, *115*, A04102. [\[CrossRef\]](#)
- Kilpua, E.K.J.; Olsper, N.; Grigorievskiy, A.; Käpylä, M.J.; Tanskanen, E.I.; Miyahara, H.; Kataoka, R.; Pelt, J.; Liu, Y.D. Statistical study of strong and extreme geomagnetic disturbances and solar cycle characteristics. *Astrophys. J.* **2015**, *806*, 272. [\[CrossRef\]](#)
- Le, G.M.; Liu, G.A. The Properties of Source Locations and Solar Cycle Distribution of GLEs during 1942–2017. *Sol. Phys.* **2020**, *295*, 35. [\[CrossRef\]](#)
- Le, G.M.; Zhao, M.X.; Li, Q.; Liu, G.A.; Mao, T.; Xu, P.G. Characteristics of source locations and solar cycle distribution of the strong solar proton events (\geq 1000 pfu) from 1976 to 2018. *Mon. Not. R. Astron. Soc.* **2021**, *502*, 2043–2048. [\[CrossRef\]](#)
- Badalyan, O.G. Spatial distribution of the N-S asymmetry of solar activity and its time variations. *Astron. Lett.* **2012**, *38*, 51–61. [\[CrossRef\]](#)
- Swinson, D.B.; Koyama, H.; Saito, T. Long-term variations in north-south asymmetry of solar activity. *Sol. Phys.* **1986**, *106*, 35–42. [\[CrossRef\]](#)
- Oliver, R.; Ballester, J.L. The north-south asymmetry of sunspot areas during solar cycle 22. *Sol. Phys.* **1994**, *152*, 481–485. [\[CrossRef\]](#)
- Joshi, B.; Joshi, A. The North-South Asymmetry of Soft X-ray Flare Index during Solar Cycles 21, 22 and 23. *Sol. Phys.* **2004**, *219*, 343–356. [\[CrossRef\]](#)
- Ballester, J.L.; Oliver, R.; Carbonell, M. The periodic behaviour of the North-South asymmetry of sunspot areas revisited. *A&A* **2005**, *431*, L5–L8. [\[CrossRef\]](#)

17. Carbonell, M.; Terradas, J.; Oliver, R.; Ballester, J.L. The statistical significance of the North-South asymmetry of solar activity revisited. *A&A* **2007**, *476*, 951–957. [[CrossRef](#)]
18. Temmer, M.; Rybák, J.; Bendík, P.; Veronig, A.; Vogler, F.; Otruba, W.; Pötzi, W.; Hanslmeier, A. Hemispheric sunspot numbers R_n and R_s from 1945–2004: Catalogue and N-S asymmetry analysis for solar cycles 18–23. *A&A* **2006**, *447*, 735–743. [[CrossRef](#)]
19. Goel, A.; Choudhuri, A.R. The hemispheric asymmetry of solar activity during the last century and the solar dynamo. *Res. Astron. Astrophys.* **2009**, *9*, 115–126. [[CrossRef](#)]
20. Li, K.J.; Gao, P.X.; Zhan, L.S. The Long-term Behavior of the North-South Asymmetry of Sunspot Activity. *Sol. Phys.* **2009**, *254*, 145–154. [[CrossRef](#)]
21. Li, K.J.; Gao, P.X.; Zhan, L.S.; Shi, X.J.; Zhu, W.W. Relative phase analyses of long-term hemispheric solar flare activity. *Mon. Not. R. Astron. Soc.* **2010**, *401*, 342–346. [[CrossRef](#)]
22. Chowdhury, P.; Choudhary, D.P.; Gosain, S. A study of the hemispheric asymmetry of sunspot area during solar cycles 23 and 24. *Astrophys. J.* **2013**, *768*, 188. [[CrossRef](#)]
23. Deng, L.H.; Qu, Z.Q.; Yan, X.L.; Wang, K.R. Phase analysis of sunspot group numbers on both solar hemispheres. *Res. Astron. Astrophys.* **2013**, *13*, 104–114. [[CrossRef](#)]
24. Feng, S.; Deng, L.H.; Xu, S.C. Long-term hemispheric variation of the flare index. *Res. Astron. Astrophys.* **2013**, *13*, 343–350. [[CrossRef](#)]
25. Deng, L.H.; Xiang, Y.Y.; Qu, Z.N.; An, J.M. Systematic regularity of hemispheric sunspot areas over the past 140 years. *Astron. J.* **2016**, *151*, 70. [[CrossRef](#)]
26. Zhang, L.; Mursula, K.; Usoskin, I. Consistent long-term variation in the hemispheric asymmetry of solar rotation. *A&A* **2013**, *552*, A84. [[CrossRef](#)]
27. Joshi, B.; Bhattacharyya, R.; Pandey, K.K.; Kushwaha, U.; Moon, Y.-J. Evolutionary aspects and north-south asymmetry of soft X-ray flare index during solar cycles 21, 22, and 23. *A&A* **2015**, *582*, A4. [[CrossRef](#)]
28. Javaraiah, J. North-south asymmetry in small and large sunspot group activity and violation of even-odd solar cycle rule. *Astrophys. Space Sci.* **2016**, *361*, 208. [[CrossRef](#)]
29. Chowdhury, P.; Kilcik, A.; Yurchyshyn, V.; Obridko, V.N.; Rozelot, J.P. Analysis of the Hemispheric Sunspot Number Time Series for the Solar Cycles 18 to 24. *Sol. Phys.* **2019**, *294*, 142. [[CrossRef](#)]
30. Roy, S.; Prasad, A.; Ghosh, K.; Panja, S.C.; Patra, S.N. Investigation of the Hemispheric Asymmetry in Solar Flare Index during Solar Cycle 21–24 from the Kandilli Observatory. *Sol. Phys.* **2020**, *295*, 100. [[CrossRef](#)]
31. Duchlev, P.I. An Estimation of the Long-Term Variation of a North–South Asymmetry of the Long-Lived Solar Filaments. *Sol. Phys.* **2001**, *199*, 211–215. [[CrossRef](#)]
32. Li, K.J.; Yun, H.S.; Gu, X.M. Hemispheric Variation in Solar Activity. *Astrophys. J.* **2001**, *554*, L115. [[CrossRef](#)]
33. Li, K.J.; Wang, J.X.; Xiong, S.Y.; Liang, H.F.; Yun, H.S.; Gu, X.M. Regularity of the north-south asymmetry of solar activity. *A&A* **2002**, *383*, 648–652. [[CrossRef](#)]
34. Singh, A.K.; Bhargawa, A. An early prediction of 25th solar cycle using Hurst exponent. *Astrophys. Space Sci.* **2017**, *362*, 199. [[CrossRef](#)]
35. Upton, L.A.; Hathaway, D.H. An Updated Solar Cycle 25 Prediction with AFT: The Modern Minimum. *Geophys. Res. Lett.* **2018**, *45*, 8091–8095. [[CrossRef](#)]
36. Jiang, J.; Wang, J.X.; Jiao, Q.R.; Cao, J.B. Predictability of the Solar Cycle over One Cycle. *Astrophys. J.* **2018**, *863*, 159. [[CrossRef](#)]